Two-Dimensional Localization with a Single Diffuse Ultrasound Field Excitation

Phillip J. White and Greg T. Clement

Abstract—**Traditional ultrasound imaging methods rely on the bandwidth and center frequency of transduction to achieve axial and radial image resolution, respectively. In this study, a new modality for spatially localizing scattering targets in a two-dimensional field is presented. In this method, the bandwidth of field excitation is high, and the center frequency is lowered such that the corresponding wavelengths are substantially larger than the target profiles. Furthermore, full two-dimensional field measurements are obtained with single send-receive sequences, demonstrating a substantial simplification of the traditional scanning techniques. Field reconstruction is based on temporal-spectral cross-correlations between measured backscatter data and a library of region of interest (ROI) backscatter data measured a priori. The transducer design is based upon a wedge-shaped geometry, which was shown to yield spatially frequency-separated bandwidths of up to 156% with center frequencies of 1.38 MHz. Initial results with these send-and-receive transducer parameters and cylindrical reflection targets in a 10-mm × 10-mm ROI demonstrate two-dimensional target localization to within 0.5 mm. Spatial localization of point scatterers is demonstrated for single and multiple scattering sites.**

I. Introduction

Ultrasound backscatter imaging in medical diagnostics is a well-established modality that uses a combination of time-of-flight measurement and beam focusing to locate objects in space [1]. Resolution along the ultrasound propagation axis is determined by the time duration of an impulsive signal, which is directly related to the signal bandwidth. Radial resolution is dictated by the ultrasound beamwidth, which is directly related to frequency. Thus, higher radial resolution images are created with higher source frequencies.

The present work examines a different approach to backscatter imaging. The method uses a reconstruction designed to resolve two-dimensional radial and axial information from a single, stationary transmitter and a single receiver. Like the traditional approach, the emitter is designed to produce an acoustic field that contains a large bandwidth. However, the field that is created is neither necessarily time-localized nor does it necessarily contain a high center frequency for achieving radial resolution. The transmitted field is not focused. Rather it achieves spatial resolution by producing a unique complex spectral signature at each point over a region of interest (ROI). Likewise, the receiver is not focused. Reflections from objects that may be within the ROI are recorded by a single receiver, and the entire ROI is reconstructed by interpretation and analysis of a single waveform.

The approach creates an acoustic field whose frequency content is spatially dependent, thus providing spatial information of a signal, recorded along a single channel in the time domain. A two-dimensional, B-mode imaging system consisting of a single transducer paired with a smaller receiving element is designed, constructed, and tested. The transducer geometry is that of a hexahedral right prism having two nonparallel surfaces, one of these being the radiating surface. The transducer, which is polarized normal to this surface, produces a radiation pattern whose complex frequency content varies with field location. The field produced by an impulsive driving potential then has a spatially-dependent amplitude and phase spectrum, which is used to reconstruct the location of scatters received by the broadband detector.

Validity of the method is dependent on the ability to perform an inverse, or pseudoinverse, operation [2], representing the separation of an object function from the signal. A cross-correlation method was investigated for performing this inversion. It was shown through simulations and experiments that these methods may be performed with the field created by the above-mentioned transducer, provided that it radiates sufficient overall transducer bandwidth, and that there is sufficient variation in the complex pressure field as a function of frequency. Two-dimensional images are assembled by cross correlating the time history of the received signal with the known response for a scatter at each location in the ROI.

The prospect of performing two- or even three-dimensional imaging with a single channel may allow higher dimensional imaging systems to be constructed with reduced electronic and emitter complexity. Because the method's radial and axial resolution are dependent on bandwidth rather than frequency, the potential also exists to perform imaging at lower overall frequencies than existing devices, which could allow application in deep or highly attenuating regions.

II. Theory

A. The Scattered Field

The proposed ultrasound emitter is a continuously driven line source that varies in frequency as a function

Manuscript received June 14, 2006; accepted July 7, 2007. Formation of this work was funded in part by NIH grants R21EB004353, U41RR019703, and 8 T32 EB02177-09.

The authors are with the Department of Radiology, Harvard Medical School, Brigham and Women's Hospital, Boston MA 02115 (e-mail: white@bwh.harvard.edu).

Digital Object Identifier 10.1109/TUFFC.2007.535

of position $\omega(\mathbf{r})$. The contribution to the overall linear pressure field from an arbitrary point at $\mathbf{r}_0$ on the source radiating into a homogeneous, space is given by:

$$p_\omega(\mathbf{r},t) = -ic_0k_0\rho_0S_\omega g_\omega\left(\mathbf{r_{S_\omega}}|\mathbf{r_0}\right), \tag{1}$$

where S_ω is the source strength, c_0 is the sound speed, ρ_0 is the density, $k_0 = \omega/c_0$, and g_ω is equal to

$$g_\omega\left(\mathbf{r_{S_\omega}}|\mathbf{r_0}\right) = \frac{e^{-ik|\mathbf{r}-\mathbf{r_0}|}}{4\pi|\mathbf{r}-\mathbf{r_0}|}. \tag{2}$$

However, if this field encounters an ROI of spatially varying density ρ and sound speed c, the time-harmonic acoustic pressure due to this point on the source then may be described by the wave equation [3]:

$$\rho\nabla\cdot\left(\frac{1}{\rho}\nabla p_\omega\right) + \frac{\omega^2}{c^2}p_\omega = 0. \tag{3}$$

It is assumed that no scattering exists outside the ROI. With the goal of expressing the field in an integral form, (3) is first multiplied by ρ_0/ρ then $-\left[\nabla^2 + \left(\omega^2/c_0^2\right)\right]p_\omega$ is added to both sides of the equation, giving the form of a harmonically driven distributed source:

$$\nabla^2 p_\omega + k_0^2 p_\omega = \nabla\cdot\left(\left\{1-\frac{\rho_0}{\rho}\right\}\nabla p_\omega\right) + \left\{k_0^2 - \frac{\rho_0}{\rho}k^2\right\}p_\omega, \tag{4}$$

which, in the absence of the scattering region, reduces to a Helmoltz equation describing p_ω in a sourceless medium. Eq. (4) may now be written in the form of a Lippmann-Schwinger integral equation [3]:

$$p_\omega(\mathbf{r}_R) = -ic_0k_0\rho_0S_\omega g_\omega\left(\mathbf{r_{S_\omega}}|\mathbf{r}_R\right) + \iiint_{\mathrm{ROI}}\left(\nabla\cdot\left(q_\rho(\mathbf{r})\nabla p_\omega\right) + q_\kappa(\mathbf{r})k_0^2p_\omega\right)g(\mathbf{r}|\mathbf{r}_R)dV, \tag{5}$$

which represents the incident wave plus the scattered wave. The function $q_\rho(\mathbf{r}) = 1-(\rho_0/\rho)$ provides a measure of the spatial variation in density, and $q_\kappa(\mathbf{r}) = 1-\left(\rho_0c_0^2/\rho c^2\right)$ is a function of variation in compressibility. If it is further assumed that the scattered field is weak, such that the first order Born approximation holds [4], the scattered pressure recorded at a point receiver located at $\mathbf{r_R}$ will be linearly dependent on the initial source function and (5) becomes:

$$p(\mathbf{r_R}) \approx ic_0k_0\rho_0S_\omega \times\left[g_\omega\left(\mathbf{r}|\mathbf{r_0}\right) + \iiint_{\mathrm{ROI}}\left[\begin{array}{c} g_\omega\left(\mathbf{r}_R|\mathbf{r}\right)\nabla\cdot\left(q_\rho(\mathbf{r})\nabla g_\omega\left(\mathbf{r}|\mathbf{r_0}\right)\right) \\ +q_\kappa(\mathbf{r})k_0^2g_\omega\left(\mathbf{r_R}|\mathbf{r}\right)g_\omega\left(\mathbf{r}|\mathbf{r_0}\right)\end{array}\right]dV\right]. \tag{6}$$

The second term in the integrand of (6) may be expanded using the standard vector identity:

$$\phi(\nabla\cdot\mathbf{A}) = \nabla\cdot(\phi\mathbf{A}) - \mathbf{A}\cdot\nabla\phi, \tag{7}$$

so that by the divergence theorem:

$$\iiint\nabla\cdot(\phi\mathbf{A})dV = \int\phi\mathbf{A}\cdot d\mathbf{S}, \tag{8}$$

where $\mathbf{S}$ is the surface surrounding the ROI, the first term in the identity given by (7) integrates to zero. Eq. (6) then becomes:

$$p_\omega(\mathbf{r_R}) \approx ic_0k_0\rho_0S_\omega \times\left[g_\omega\left(\mathbf{r}|\mathbf{r_0}\right) + \iiint_{\mathrm{ROI}}\left[\begin{array}{c} q_\rho(\mathbf{r})\nabla g_\omega\left(\mathbf{r}_R|\mathbf{r}\right)\nabla g_\omega\left(\mathbf{r}|\mathbf{r_0}\right) \\ +q_\kappa(\mathbf{r})k_0^2g_\omega\left(\mathbf{r_R}|\mathbf{r}\right)g_\omega\left(\mathbf{r}|\mathbf{r_0}\right)\end{array}\right]dV\right]. \tag{9}$$

The point receiver will simultaneously receive the integral sum of the pressure due to all points on the source $\mathbf{r}_0$. The scattered acoustic pressure at $\mathbf{r_R}$ then will be time dependent as described by:

$$p\left(\mathbf{r_R},t\right) = \sum_{\mathbf{r_0}}\iiint_{\mathrm{ROI}}\left[q_\rho(\mathbf{r})P_\rho\left(\mathbf{r_R},\mathbf{r},\mathbf{r_0}\right) + q_\kappa(\mathbf{r})P_\kappa\left(\mathbf{r_R},\mathbf{r},\mathbf{r_0}\right)\right]e^{i\omega(\mathbf{r_0})t}dV, \tag{10}$$

where the kernels $P_\rho\left(\mathbf{r_R},\mathbf{r},\mathbf{r_0}\right)$ and $P_\kappa\left(\mathbf{r_R},\mathbf{r},\mathbf{r_0}\right)$, having the dimension of pressure per unit volume, are obtained by combining terms in (9).

B. Image Reconstruction

The task at hand is to search for solutions of the scattering functions $q_\rho(\mathbf{r})$ and $q_\kappa(\mathbf{r})$ in (10), assuming that the field transmitted from the transducer, and thus $P_\rho\left(\mathbf{r_R},\mathbf{r},\mathbf{r_0}\right)$ and $P_\kappa\left(\mathbf{r_R},\mathbf{r},\mathbf{r_0}\right)$ are known. To produce a source whose frequency response varies linearly along the length of the source aperture, a single crystal emitter is proposed that has the shape of a hexahedral right prism or "doorstop" shape. Similar geometries have been proposed for scanning ultrasound beams by emitting a single frequency at a given time, achieving wider bandwidth [5], and for increasing the overall bandwidth of a transducer [6], but not for the present purpose of producing a divergent broadband beam, with a complex field profile. In practice, the transducer would be air backed to provide maximum quality factor (Q) at a giving point on the transducer, and the transducer would be powered by an impulsive signal with a time duration much shorter ($< \times\, 0.1$) than that of the period of the highest radiating frequency and with a repetition frequency equal to or lower than that of the lowest radiating frequency. Incidentally, it is interesting to note that, even in the ideal case in which the transducer is continuously driven, the amplitude peaks are time limited. A numeric example of such a signal is provided in Fig. 1.

The field produced by the impulsively-driven transducer is scattered and received by a point receiver. Due to the profile of the transmitted field and the spatial sensitivity of the receiver itself, the spatial sensitivity will depend highly on the receiver's position relative to the transducer, as shown in Fig. 2. The boxed area in front of the transducer in Fig. 2 indicates a region with relatively flat sensitivity that would qualify as the ROI. If a scattering field were

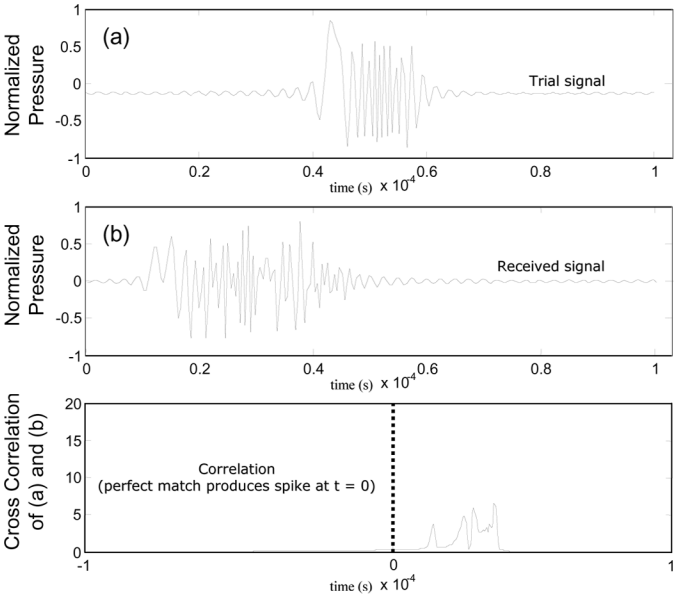

Fig. 1. Simulated sequence of the method: a time-limited excitation signal (top), a time-extended scattered signal (center), and the cross correlation of the two signals (bottom).

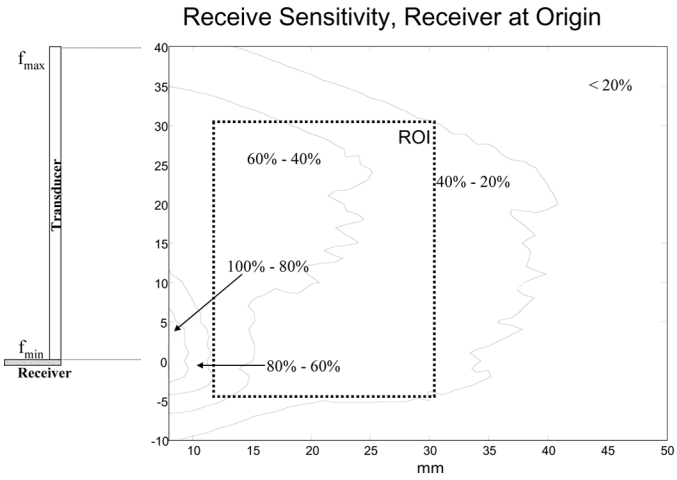

Fig. 2. Contours of the peak amplitude as a function of position in front of the emitting transducer, assuming equal-strength scattering at all points. The sensitivity also will depend on the receiver position. Here the ROI is selected as a rectangular area with amplitude variation between 20% and 60% of the peak.

located within this region, a time-extended signal would be received, as illustrated in Fig. 1.

Once this single waveform is received, it may be processed to solve for q_s. The problem is approached by developing a high-resolution database of the signal $p_Q(\mathbf{r_R}, t)$ as a function of position due to a single point scatterer $Q(\mathbf{r})$ located within an otherwise homogeneous ROI. This response could be measured by scanning a point-like scatterer through the ROI or, alternatively, it could be calculated for scatterers of varying density and compressibility. A cross correlation between this signal and the expected response $p_Q(\mathbf{r_R}, t)$ then is calculated for each point in the ROI according to:

$$I_{Q(\mathbf{r})}\left(t', \mathbf{r_R}\right) = \int_{-\infty}^{\infty} p_{Q(\mathbf{r})}\left(\mathbf{r_R}, t\right) p\left(\mathbf{r_R}, t + t'\right) dt. \tag{11}$$

By the property of the correlation integral, first order scattering would produce a peak at $t = 0$ provided that part of $p_Q\left(\mathbf{r_R}, t\right)$ is superimposed in $p\left(\mathbf{r_R}, t\right)$. Thus, the cross correlation at $t = 0$ is selected as the image intensity at $\mathbf{r}$. The process is repeated for each position $\mathbf{r}$ over the ROI to form an image.

III. Materials and Methods

A. Simulation

Simulation of the acoustic pressure at the receiver was performed using a discrete approximation to the Rayleigh-Sommerfeld integral:

$$p_R(t) = \sum_Q \sum_S \left[q_\kappa \frac{e^{ik_s r_s}}{r_s} + q_\kappa \frac{e^{ik_s r_s}}{r_s} \right] \frac{e^{ik_s r_R}}{r_R} e^{i\omega_s t} \Delta S \Delta R, \tag{12}$$

where S is a section of the surface area of the transducer and R is the scattering cross section of the scattered field. The transmission transducer face was situated in the Cartesian y-z plane, symmetric about the y-axis. In all simulations, the emitting transducer length was situated along the y-axis, and the receiver was point-like and could be located at arbitrary points in space. The resonance frequencies varied linearly along the length of the radiating face. For the calculation of (12), the transducer surface was divided into squares with dimensions equal to one-quarter wavelength of the highest frequency for a given transducer.

Image construction was performed as described in Section II-B. This process is illustrated conceptually in Fig. 1, showing a signal at the receiver and a trial signal, indicating the unique, or nearly unique, waveform produced by scattering from a specific point in the ROI. Continuously-driven transducers were modeled with linearly varying frequencies. The ROI contained a planar scattering field $q_\kappa(\mathbf{r})$, situated in the imaging plane.

B. Transducers

Two prototype transducers were constructed and used for this study: one was cut from a 25 mm × 15 mm × 4.4 mm (length × width × thickness) PZT-4 crystal (Transducer A), and the other was cut from a 38 mm × 10 mm × 8.0 mm (length × width × thickness) PZT-4 crystal (Transducer B). The transducers were all electrically poled to operate in their thickness modes, at their fundamental frequencies of 0.5 MHz (Transducer A) and 0.25 MHz (Transducer B). In each case, the crystals were cut diagonally through the thickness dimension using a diamond-wire saw. The cut crystals then were mounted in machined acrylic housings such that they were air backed with their radiating surfaces electrically grounded. Two layers of conductive

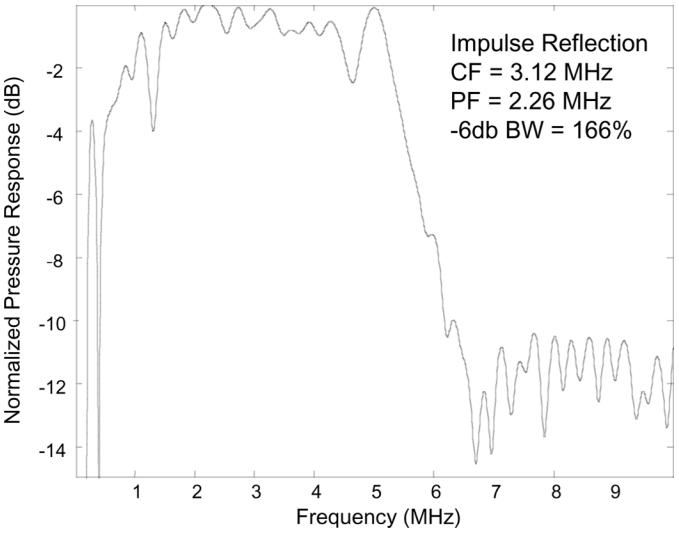

Fig. 3. Normalized pressure response of Transducer A as obtained with impulse-reflection (CF = Center Frequency, PF = Peak Frequency, BW = Bandwidth).

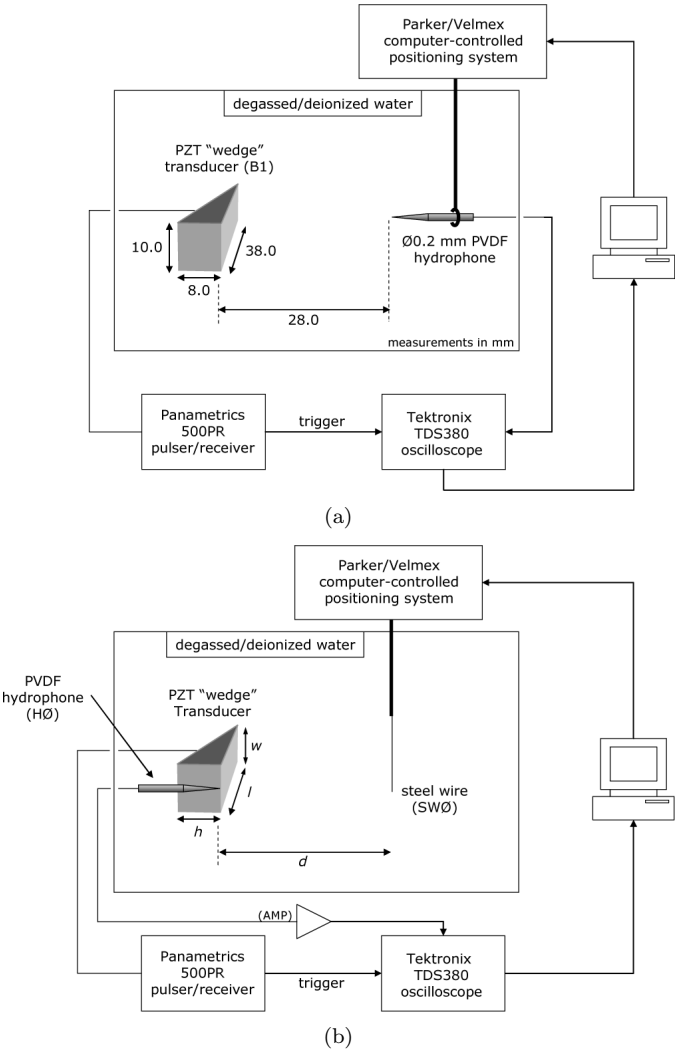

Fig. 4. (a) Experimental setup for scanning the pressure field of Transducer B. (b) Experimental setup for field scanning with a copper wire target. For Transducer A scanning, the parameters were $l = 25.0$ mm, $w = 15.0$ mm, $h = 4.4$ mm, $d = 15.0$ mm, SWØ = 0.2 mm, HØ = 0.5 mm, and AMP = +25 dB. For Transducer B scanning, the parameters were $l = 38.0$ mm, $w = 10.0$ mm, $h = 8.0$ mm, $d = 45.0$ mm, SWØ = 0.13 mm, HØ = 2.0 mm, and AMP = +30 dB.

epoxy (Mereco, West Warwick, RI) were applied to the cut surfaces and wired as the actuation electrode.

The frequency response of Transducer A was measured by analyzing the results of an impulse-reflection signal. The transducer was actuated by broadband spike excitation (Panametrics, Waltham, MA, model 500PR) and the signal was reflected from a submerged planar steel target oriented perpendicular to the transducer's axis of propagation. The reflected time signal, as received by the same transducer, was Fourier transformed to yield a frequency response of the transducer (Fig. 3). The −6 dB bandwidth was measured to be 166%, with a center frequency of 3.12 MHz and a peak frequency of 2.26 MHz.

The radiation field frequency content of Transducer B was experimentally determined via three methods within the ROI pertinent to this study. First, a two-dimensional pressure scan of the radiated field was performed with a 0.2-mm diameter PVDF probe [Fig. 4(a)]. As the transducer was actuated by broadband spike excitation, the pressure probe, in conjunction with a computer-controlled positioner (Parker, Hannifin, PA) and oscilloscope system (Tektronix, Beaverton, OR, model TDS380), recorded a 20-μs sequence of measured pressure for each point in a spatial Cartesian grid. The scan was performed for a 40 mm × 40 mm plane (1-mm measurement resolution) centered 28 mm from the face of the transducer and oriented parallel to the length dimension of the transducer. Using Matlab (The MathWorks, Natick, MA), these measured time-pressure sequences were separated in frequency, and plotted in grayscale to demonstrate the asymmetric and varied nature of the spatial energy distribution. Results for the amplitude and phase of the 2.0-MHz, 4.0-MHz, and 6.0-MHz cases are shown in Fig. 5. The peak-to-peak maximum pressures and relative phases for the composite field are shown in Fig. 6.

A second method to characterize the transducer was based on an impulse send-receive technique in which a spiked excitation would be propagated and reflected from a near-perfect reflector. The reflected signal then would be received by the same transducer and analyzed. With a setup similar to that shown in Fig. 4, Transducer B was actuated with a spike, the resulting pressure wave was propagated 14 mm to a planar water-air interface, then the reflected signal received by the same transducer. The time signal then was analyzed to yield a frequency-dependent pressure response as shown in Fig. 7. With this method, the −6 dB bandwidth was measured to be 120%, with a center frequency of 1.45 MHz and a peak frequency of 1.63 MHz.

A third measurement of the frequency response of Transducer B was based upon a radiation force effect, in which the force exerted by a propagating ultrasound wave onto a perfectly absorbing target is in direct pro-

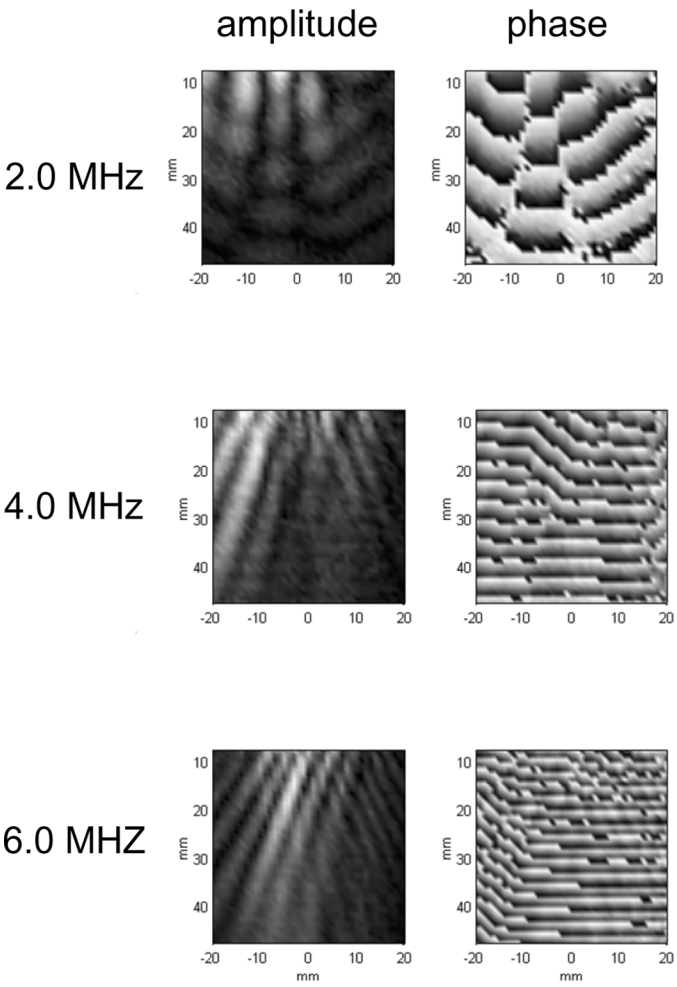

Fig. 5. Three representative frequency-isolated pressure magnitude and phase fields of the impulse radiation of Transducer B.

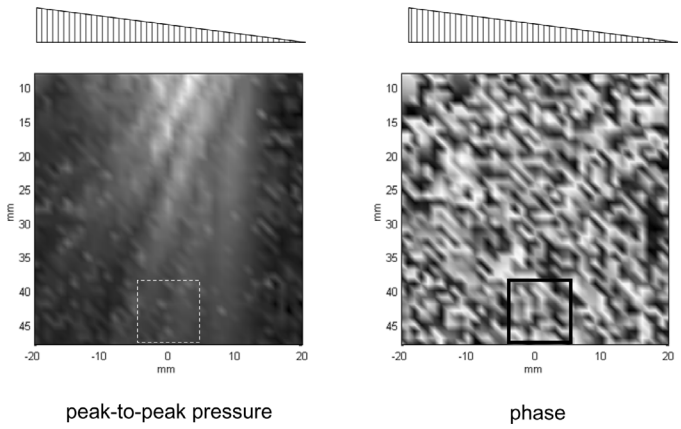

Fig. 6. Radiated pressure magnitude and phase fields of Transducer B. The position and orientation of the transducer are indicated by the wedge-shaped blocks above the plots. The vertical hash marks within these blocks are parallel to the piezoelectric polarization direction of the PZT crystal. The dashed and solid boxes set within the radiated field delineate the ROI for experiments performed with this transducer.

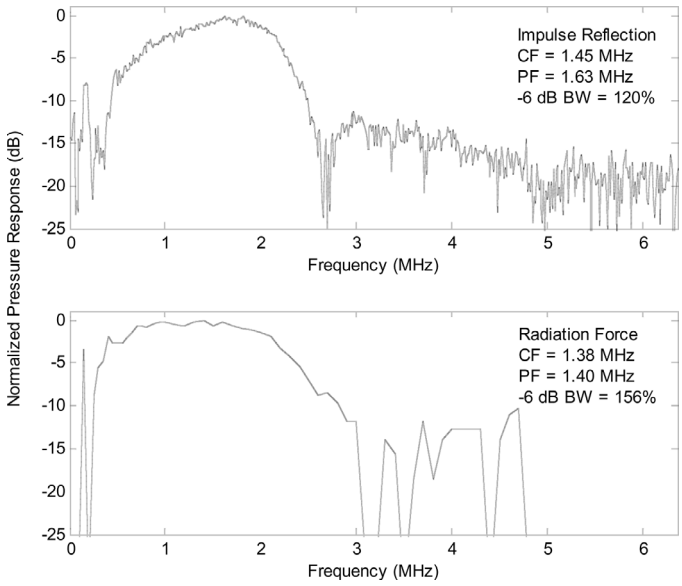

Fig. 7. Impulse response of Transducer B as measured by impulse-reflection (top) and radiation force (bottom) (CF = Center Frequency, PF = Peak Frequency, BW = Bandwidth).

portion to the impinging acoustic energy [7]. The transducer was positioned to direct its beam into an absorbing target, which was coupled to a digital force balance (Mettler Toledo, Columbus, OH, model PR2003DR). The output power of the transducer, driven with continuous-wave actuation, was measured from 0.1 MHz to 7.0 MHz. The results also are plotted in Fig. 7. The radiation force measurement yielded a −6 dB bandwidth of 156%, with a center frequency of 1.38 MHz and a peak frequency of 1.40 MHz.

C. Experiments

For the first experiment, Transducer A was mounted in a rubber-padded tank filled with deionized water [Fig. 4(b)]. A 0.5-mm diameter PVDF hydrophone (Precision Acoustics, Dorchester, UK) situated directly next to the transducer served as the receiver. To obtain scattering $p_Q(\mathbf{r_R}, t)$ as a function of position, a vertically-oriented 0.2-mm diameter copper wire was guided to arbitrary positions in the tank using a stepper-motor-controlled three-dimensional positioning system (Velmex, Bloomfield, NY). The wire targets for all experiments were 102 ± 5 mm in length, attached at the ends to a polymer mount by silicone adhesive/sealant. The distance between the mounts (102 ± 5 mm) was an order-of-magnitude larger than the measured vertical beamwidth of the transducers (−6 dB pressure at 6.0 ± 0.5 mm), ensuring negligible backscatter signals. In addition, because the transducer-target distance was substantially smaller than the transducer-mount distance, any backscatter not arising from the wire targets would be outside of the measured time window. The response of the hydrophone was sent through an amplifier and recorded by an oscilloscope (Tektronix, Beaverton, OR). The wire positioning and data acquisition were both computer controlled. The wire was scanned over a 30 mm × 20 mm area in front of the transducer, with waveforms from the hydrophone recorded at 0.2-mm inter-

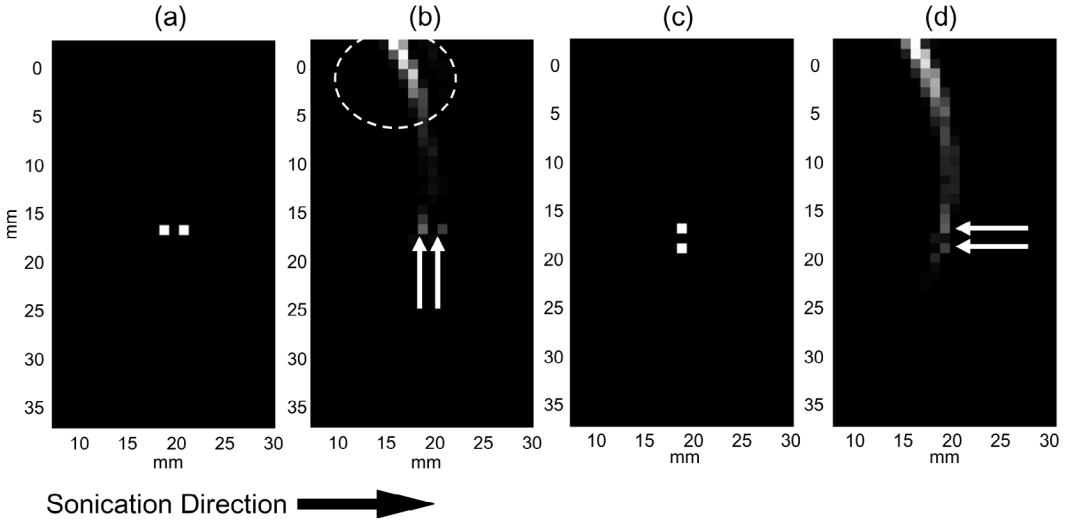

Fig. 8. Simulations for two 0.25-mm scatters in the ROI placed with (a) 1-mm separation orthogonal to the transducer surface and (b) the reconstructed ROI. Arrows indicate the objects, with an encircled reconstruction artifact. (c) and (d) Similarly, the scatters parallel to the transducer can be individually detected after 2-mm separation, but again, with artifact.

vals. The center of this scanned area was located approximately 15 mm in front of the transducer. Following this measurement, objects were placed in front of the transducer, and the waveforms were recorded again. This set of single waveforms was processed by calculating the cross correlation presented in (11) for each point in the ROI scanned with the wire.

The second experiment explored the proposed imaging modality with a lowered center frequency of field excitation and a smaller scattering target. Transducer B was positioned in the experimental setup as diagrammed in Fig. 4(b). A 0.13-mm diameter copper wire, which was coupled to and positioned by a stepper-motor-controlled positioning system, was guided throughout an ROI with relatively high sensitivity (Fig. 6). For each location of the wire, which was sequentially positioned in Cartesian coordinate positions throughout a 10 mm × 10 mm planar area in 0.5-mm increments, a 20-μs time sequence of the received signal, including the reflection from the wire target, was recorded. The scanned field was centered 45 mm from the face of the transducer. This scan was repeated twice for the same field, and the results were averaged at each spatial location to reduce noise artifacts. Next, copper wire targets were placed in various locations within the ROI, and a single 20-μs time sequence of each reflected signal was recorded. Each of the waveforms, corresponding to various placements of scattering sites, then was sequentially cross correlated according to (11) with each saved waveform from the composite scans of the field. The results of the cross correlations then were analyzed to determine the accuracy in reproduction of the scattered field.

IV. Results

A. Simulation

Simulations were performed to calculate the pressure field and received signal from a 40 mm × 10 mm planar transducer with linear frequency variation between 0.3 MHz and 2.5 MHz over its length. A point-receiver with a flat frequency response over relevant range was situated at the low frequency end of the transducer, and centered about its width. Both the surface dimensions and frequency range were selected to approximate the radiation behavior of Transducer B. An ROI was selected in an area in front of the transducer between the distances of 10 mm to 30 mm normal to the transducer surface and −5 mm to 35 mm along its length.

Simulated results verified the ability of the method and present geometry to detect and localize one or more scatters within the ROI under idealized conditions. All scatterers in the ROI were assigned a scattering strength of $q_\kappa = 0.1$, caused by a speed of sound increase from 1.50×10^3 ms^{-1} to 1.58×10^3 ms^{-1}. With the present geometric and frequency configuration, localization was evident in both the axial and radial direction of a 0.25-mm diameter object at or below the range of wavelengths in the signal (0.60 mm to 5.0 mm). This indicated the ability to image subwavelength scatterers without the characteristic blurring associated with backscattered ultrasound detection. The separation between two or more 0.25 mm-diameter scatterers placed at least 1 mm apart was also possible with the low frequency emitter. In a series of images that moved to objects successively further from each other (simulated at 1-mm intervals), a 1-mm separation was detectable along the normal axis [Fig. 8(b)], and 2-mm separation could be detected along the transducer length [Fig. 8(d)]. However, in both of these simulations, as well as subsequent simulations with multiple objects, reconstruction artifacts appeared in the images, as indicated by the dotted outline in Fig. 8(b).

B. Experiment

Three examples of the resulting measured field analyses are presented in Fig. 9 for scans performed with Trans-

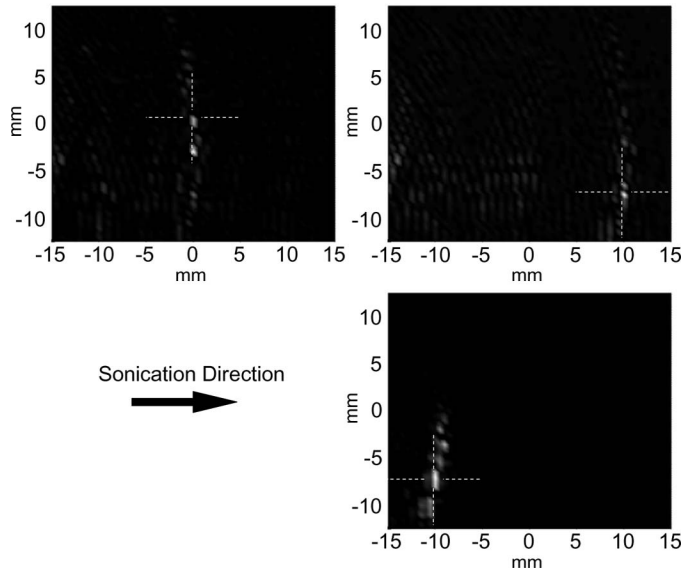

Fig. 9. Cross-correlation fields for three placements of scattering targets using Transducer A as the excitation source and a 0.5-mm diameter, pressure-sensitive hydrophone as the detector. The intersections of dashed crosshairs indicate the actual positions of scatterers.

ducer A. Relative to the images, the transducer was situated to the left, with the thick portion ($f_{\min}$) toward the bottom. The cross-correlation analyses of these scans yielded high correlations at the field location corresponding to the locations of scatterers, marked by the intersection of the dashed crosshairs in each panel of Fig. 9. The grayscale intensities in these images were set to be proportional to the degree of correlation at the origin of the cross-correlation analysis, as diagramed in Fig. 1. In addition, a linear interpolation filter was applied between adjacent pixels. In each scan, there was evidence of correlation artifacts, predominantly in the radial direction of the images (i.e., orthogonal to the propagation axis of the transducer).

Similar scans then were performed using Transducer B. The aim of this portion of the study was, in part, to examine the feasibility of using an excitation source of substantially lowered center frequency to localize scatterers of reduced geometry. Within the ROI for these scans (Fig. 6), it was evident that the complex pressure field spatial distribution is asymmetric and irregular, not only in magnitude, but also in phase. This asymmetry gave assurance that the complex backscatter at each point within an ROI would have a unique value. The scatterers in this case were copper wires with measured diameters of 0.13 mm, and the excitation center frequency had a wavelength in water of 1.1 mm (calculated using 1.38 MHz, the center frequency as measured by the radiation force method and a sound speed in water of 1500 ms^{-1}).

Four examples of analyzed scatter fields for single targets are shown in Fig. 10. In these images, the source transducer is situated to the bottom of the diagram with the thick portion ($f_{\min}$) toward the right, and the receive hydrophone is situated 10-mm to the right of the excitation transducer. The results of the cross-correlation analyses revealed a spatial correlation between the measured and actual scatter site to within 0.5 mm for single scatterers. In Fig. 11, three examples are shown for a series of field reconstructions for single excitation of a field with simultaneous two point scatterers, each with diameters of 0.13 mm. These measurements were performed with the same experimental setup and reconstruction algorithm as those of Fig. 10. The localization of two distinct scatterers was to within 0.5 mm; and, although there are artifacts, the contrast was sufficient to identify the scatter sites.

V. Discussion

This study was devised to determine whether a single sonicate-receive sequence can be used to localized backscatter signals not only along the ultrasound axis of propagation, but also along the radial direction. Initial simulations suggested that it is possible, provided that the sonicating transducer has sufficient bandwidth. A key finding of the simulation study was that even relatively low bandwidths were able to detect and localize small, point-like objects. But the ability to detect a signal degraded with increasingly complex signals. Based on these numeric results, transducers with varied excitation and reception parameters were constructed to test in an experimental setup. These experiments, in general, supported the simulated cases.

For the first experiment, in which Transducer A was the field excitation source and a needle hydrophone was the receiver, a limiting factor was the diameter of the hydrophone relative to the wavelengths emitted from the source transducer. The underlying assumption of a point receiver is that its surface area is much smaller than the received wavelengths, which is clearly not the case for this preliminary work. However, it was still able to perform two-dimensional localization of scattered objects, albeit with the introduction of interference artifacts in the images. The predominance of artifacts in the radial directions, rather than the axial directions, implied that the temporal isolation of the backscattered signal gives a higher localizing value than the spectral signature. These two observations (i.e., the obviation of a small receiver and the necessitation of a wider spectral spread) led, in part, to the design of the second set of experiments with Transducers B.

The design parameters and implementation strategies of Transducer B were intended to address two feasibility issues: first, whether a lowered center frequency of operation would preclude possibility of submillimeter localization resolution in distal regions of an image field; and second, whether a wider bandwidth would reduce artifacts in the radial direction of imaging. A transducer geometry with a larger thickness dimension, and tapered linearly to zero, was hypothesized to give a lower center frequency and higher bandwidth than one with a smaller thickness dimension. In this study, Transducer B had a thickness

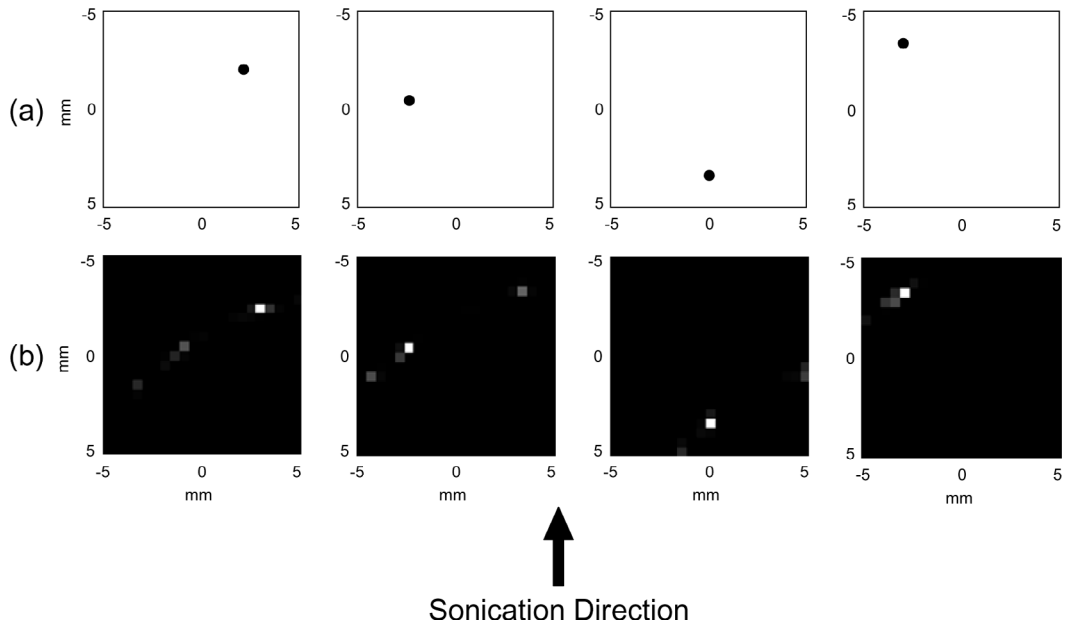

Fig. 10. Cross-correlation fields for four placements of scattering targets using Transducer B as the excitation source, and a 2.0-mm diameter, pressure-sensitive hydrophone as the detector. The panels of row (a) indicate the actual positions of the scatterers in the ROI and the corresponding field reconstructions are shown directly below in row (b).

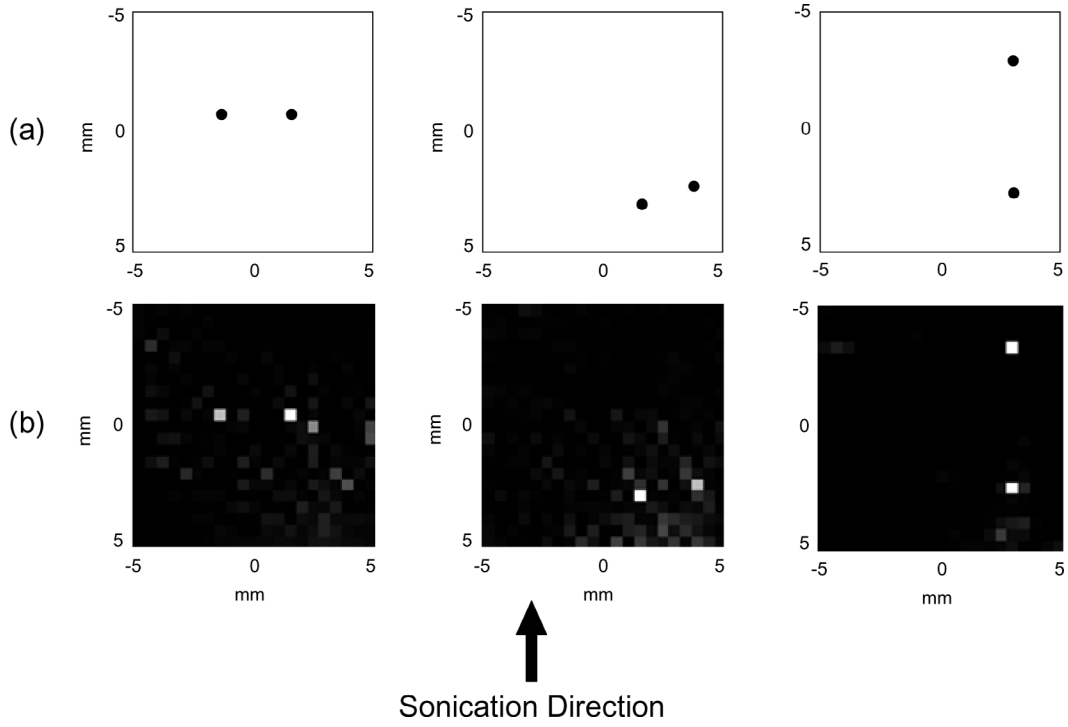

Fig. 11. Cross-correlation fields for three placements of two scattering targets using Transducer B as the excitation source and a 2.0-mm diameter, pressure-sensitive hydrophone as the detector. The panels of row (a) indicate the actual positions of the scatterers in the ROI and the corresponding field reconstructions are shown directly below in row (b).

that was nearly twice that of Transducer A. The characterization of Transducer B confirmed a lowered center frequency (1.67 MHz lower than Transducer A); but, contrary to the hypothesis, the bandwidth also was measured to be reduced (from 166% to 120%). These parameter comparisons between Transducer A and Transducer B were made using the parameters as obtained from impulse reflections. The radiation force measurements performed with Transducer B yielded a 36% larger bandwidth and a 0.07 MHz lower center frequency than that of the impulse reflection measurement. The discrepancy possibly arose from out-of-field, low-frequency scattering in the impulse reflection setup. Nonetheless, with each measurement method, Transducer B was shown to operate at a lowered center frequency and a slightly reduced bandwidth.

The results of image reconstructions from scans performed with Transducer B were able to address the issue of submillimeter localization in distal regions. Yet, it also confirmed the existence of radial artifacts for transducer bandwidths between 120% and 166% and center excitation frequencies of 1.38 MHz to 3.12 MHz. The data, however, demonstrated that spatial localization resolutions substantially lower than the excitation wavelengths can be expected, even when the wavelength of the center excitation frequency is an order-of-magnitude larger than the scattering targets' spatial dimensions. Even for the highest efficiently radiating frequency (2.45 MHz), the corresponding wavelength was more than four times that of the scattering profile. It also was demonstrated that receiver size, relative to wavelength, did not present an impediment to this localization method. In this case, compared qualitatively with the results of experiments performed with Transducer A, signal integration across a larger receiver diaphragm had a negligible effect on the preservation of a unique backscatter signature. When more than one scatterer was introduced into the ROI, accurate localization also was achieved.

VI. Summary

A numeric and experimental study investigated an approach toward creating a two-dimensional image from a single recorded time trace. A transducer design that created a diffuse frequency-separated ultrasound field was used to demonstrate feasibility. The concept was rooted in acoustic scattering theory, coupled with the Born approximation, such that weak scatterers in a frequency-separated acoustic field scattered linearly, retaining a unique complex frequency signature. The scattered field, in theory, could be analyzed for both spectral and temporal content, revealing enough information to localize scatter sites in three-dimensional space. With the present transducer designs, target localization with single time traces was shown for single and multiple scatterers in two-dimensional imaging fields.

That target localization could be achieved with excitation wavelengths substantially larger than the individual scattering profiles was a key finding. This implication of a potential for relatively high resolution imaging at lowered frequencies motivates further studies in highly attenuating media. A study is being conducted to apply this method for an intraoperative transcranial monitor. The demonstrated ability to localize in two dimensions with a lowered frequency would be an asset to its application through the highly absorbing skull bone. Also, with better transducer design and field analyses algorithms, the potential for fine resolution imagery in attenuating soft tissues and within deep-set ROI can be achieved.

References

[1] B. B. Goldberg and B. A. Kimmelman, *Medical Diagnostic Ultrasound: A Retrospective on its 40th Anniversary*. Rochester, New York: Eastman Kodak Company, 1988.

[2] W. H. Press, S. A. Teukolsky, W. T. Vetterling, and B. P. Flannery, "Integral equations and inverse theory," in *Numerical Recipes in C: The Art of Scientific Computing*. 2nd ed. New York: Cambridge University Press, 1992, pp. 788–826.

[3] P. M. Morse and K. U. Ingard, *Theoretical Acoustics*. Princeton, NJ: Princeton Univ. Press, 1968.

[4] W. Tobocman, D. Driscoll, N. Shokrollahi, and J. A. Izatt, "Free of speckle ultrasound images of small tissue structures," *Ultrasonics*, vol. 40, no. 9, pp. 983–996, 2002.

[5] F. L. Lizzi and W. Weil, "Frequency-controlled scanning of ultrasonic beams," U.S. Patent 43509172, Jun. 9, 1980.

[6] K. Ustuner, "Frequency and bandwidth controlled ultrasound transducer," U.S. Patent 605763, May 2, 2000.

[7] K. Hynynen, "Acoustic power calibrations of cylindrical intracavitary ultrasound hyperthermia applicators," *Med. Phys.*, vol. 20, pp. 129–134, Jan. 1993.